

Inter-granular cracking through strain gradient crystal plasticity and cohesive zone modeling approaches

T. Yalçinkaya^{a,*}, İ. Özdemir^b, A.O. Firat^a

^a Department of Aerospace Engineering, Middle East Technical University, Ankara 06800, Turkey

^b İzmir Institute of Technology, Department of Civil Engineering, 35430 Urla, İzmir, Turkey



ARTICLE INFO

Keywords:

Strain gradient plasticity
Cohesive zone modeling
Fracture
Inter-granular crack
Polycrystalline plasticity

ABSTRACT

Even though intergranular fracture is generally regarded as a macroscopically brittle mechanism, there are various cases where the fracture occurs at the grain boundaries with considerable plastic deformation at the macroscopic scale. There exists several microstructural reasons for grain boundaries to host crack initiation. They can interact with impurities and defects, can provide preferential location for precipitation, can behave as a source of dislocations and can impede the movement of dislocations as well. The understanding of the crack initiation and propagation at the grain boundaries requires the analysis of the grain boundary orientation and the orientation mismatch between the neighboring grains and the related the stress concentration, which is only possible through the combination of micro-mechanical plasticity and fracture mechanics. For this reason the current work studies the evolution of plasticity in three dimensional Voronoi based microstructures through a strain gradient crystal plasticity framework (see e.g. Yalçinkaya et al., 2011; Yalçinkaya et al., 2012; Yalçinkaya, 2016) and incorporates a potential based cohesive zone model (see Park et al., 2009; Cerrone et al., 2014) at the grain boundaries for the crack initiation and propagation. The numerical examples considers the effect of the orientation distribution, the grain boundary conditions, the specimen size and the fracture energy parameter on the intergranular fracture behavior of micron-sized specimens. The study presents important conclusions for the modeling of fracture at this length scale.

1. Introduction

In recent years the production of miniaturized products has become a global trend in various industrial clusters such as, electronics, communication, aerospace, biomedical devices, defense and automotive, which requires advanced manufacturing technologies at micron level (see e.g. [1,2]). Various challenges, such as size effect and stress concentrations at the grain boundaries, arise at the grain scale. In other words, during plastic deformation of micron-sized metallic products, the material homogeneity assumption does not work anymore. Therefore, crack initiation and propagation are rather dominated by local maximal values around grain boundaries or interfaces (see e.g. [3–5]). Various metallic alloys, e.g. aluminum, exhibit substantial localization and stress concentration at the grain boundaries. In this regard, intergranular damage evolution, crack initiation and propagation becomes an important failure mechanism at this length scale. Our recent experimental studies in micron sized Al 6061-T6 specimens, using micro DIC technique, illustrated that localization mainly occurs at the grain boundaries under uniaxial tension and at both grain boundaries and

grain interiors under equibiaxial tension conditions [5]. Moreover it was observed that it is quite difficult to validate crystal plasticity simulations with micro DIC observations in specimens having 50–100 grains without an interface model handling the localization and cracking at the grain boundaries. Occurrence of intergranular microcracks at this length scale, influences the performance of many alloys at macro scale as well.

One class of material that is commonly referred to for the ductile grain boundary failure is the high strength aerospace aluminium alloys (Al-Zn-Mg-Cu-Cr), having intra- and intergranular precipitation due to heat treatment. Such materials have low fracture toughness due to intergranular fracture (see e.g. [6,7]). The grain boundary microstructure classically exhibits a Precipitate Free Zone (PFZ) and grain boundary precipitates. The typical behavior of the PFZ/grain boundary after heat treatment will be a low yield stress and a high work hardening rate. The PFZ is considered to be the soft location deforming first and it is constrained by the elastic grains imposing high stress triaxiality. This activity leads to large void growth rate and rapid coalescence leading to intergranular cracking. In certain cases the stress inside the grains

* Corresponding author.

E-mail address: yalcinka@metu.edu.tr (T. Yalçinkaya).

<https://doi.org/10.1016/j.tafmec.2019.102306>

might reach to yield stress before the onset of coalescence in the PFZ, dropping the triaxiality in the PFZ due to its higher hardening capacity. Then the voids tend to grow inside the grain. Due to the low hardening capacity of the grain, a state of damage induced softening is rapidly attained until voids finally coalesce within the grain. This point of view explains the intergranular and trans-granular ductile fracture mechanisms in the continuum length scale. There have been a number of models developed at continuum scale to address the micromechanical features of failure (see e.g. [8–11]). Even though there are several important conclusions through such phenomenological models, a further improvement on the occurrence of failure modes in ductile materials as a function of the relevant microstructural parameters is required [9], which is basically the scope of the current work.

As a good candidate material for aerospace applications, the Ti β alloy, experiences the same problem as well with the fracture toughness. This class of materials is attractive because of their density-normalized strength. However, their current use is limited because they are prone to room temperature grain boundary ductile fracture that reduces their ductility and/or fracture toughness, thus limiting their usefulness in fracture-critical structures (see [12]). Therefore, these lightweight alloys are often excluded as an option, yet their failure mechanisms should be studied to quantify the factors that cause grain boundary ductile fracture. Then their usage at the critical components such as landing gear could be discussed further. Due to their high strength at room temperature, high-temperature forming has become an effective approach for manufacturing complex structured components of titanium alloys. Yet, microcracks may initiate and propagate in the material, which will result in GB fracture or interior fracture that weakens the fatigue life of the component. Grain boundaries contribute significantly to the microcracks because that GBs become the weakest region during the high temperature deformation, and so the deformation, damage and fracture of GBs may directly cause plasticity enhancement, microcrack initiation and propagation, respectively (see [13]).

The general microstructural understanding elucidates that intergranular fracture occurs predominantly along the high angle grain boundaries. In other words, the chance of intergranular fracture increases with the misorientation. The nucleation of intergranular cracks is attributable to dislocation pileup at high angle grain boundaries (see [14–17]). The large grain size of the recrystallized grains (25–100 μm) facilitates the dislocation pileup and, consequently, the stress concentration at these boundaries. The slip transfer across these boundaries is difficult because of the presence of coarse incoherent η precipitates and the high angle nature of the boundaries. These factors facilitate nucleation of intergranular cracks. Therefore, the length scale of the intergranular fracture phenomenon requires the usage of micro-mechanically motivated models that intrinsically take into account the crystallographic information affecting naturally the crack initiation and propagation as well as the decrease in the fracture toughness. A number of studies addressed the phenomenon through constitutive models at molecular and grain scale (see e.g. [18–23]) mostly coupled to certain interface models. However the studies in the literature are quite restricted. The models are mostly local and the description of the grain boundary conditions is not possible, which is crucial. Moreover the size effect, grain boundary localization and the effect of the grain orientation and the mismatch could not be predicted.

Most commonly used local crystal plasticity finite element simulations of polycrystalline materials can capture the strain localization due to orientation mismatch. However, they lack any kind of grain boundary-dislocation interaction information, and give jumps at the grain boundaries. On the other hand the non-local (strain gradient) crystal plasticity approaches offer the possibility of defining grain boundary conditions and they can handle the localizations in a much smoother way (see e.g. [24–26]). The grain boundary conditions influence the localization substantially. These conditions might define the physical mechanisms resulting in complete blockage of dislocations or

free transition through grain boundaries. For the crack initiation modelling a special treatment of the grain boundaries is required, which is done here through the insertion of potential based cohesive zone elements between the grains (see [27,28]). In this context, the purpose of the current work is to conduct a physical analysis of intergranular fracture by combining the strain gradient crystal plasticity and the cohesive zone modelling techniques in order to simulate the grain size, orientation mismatch and grain boundary condition dependent crack initiation and propagation, which makes it a unique study compared the existing ones in the literature. Virtual microstructures are prepared in 3D through Voronoi tessellation and the computations are conducted in Abaqus through UEL subroutines. The pre- and post-processing of the simulations are automated through developed scripts and important conclusions are obtained from the study. The developed study offers a great potential to be used in realistic simulations of plasticity and inter-granular cracking in micron sized specimens. Since the developed models, routines and scripts are incorporated in a commercial software, it is quite easy to use as well.

The paper is organized as follows. First, in Section 2, the rate dependent strain gradient crystal plasticity and its finite element solution is briefly discussed. Then, in Section 3, the incorporation of the potential based cohesive zone elements is presented. In Section 4, numerical examples are presented in order to demonstrate the capability of the proposed model. First, the orientation distribution dependent intergranular fracture phenomena is discussed. Then the effect of the grain size, grain boundary condition and the fracture energy parameter on the crack initiation is addressed. Finally, some concluding remarks are given in Section 5.

2. Rate dependent strain gradient crystal plasticity

Two computational models for plasticity and fracture are used together in this study in order to simulate the intergranular fracture phenomenon at grain scale. The first model is the rate dependent strain gradient crystal plasticity framework (see e.g. [24,29,30]), which runs for the simulation of bulk grain behavior. The model is extended to 3D here and implemented as UEL subroutine in Abaqus software. The constitutive model has actually been developed originally as a non-convex model for deformation patterning modelling in single crystals. In here, the convex counter-part of the model is employed to predict the size dependent nonlocal behavior of metallic materials. Even though the gradient nature of the crystal plasticity model makes it complicated to implement, the formulation is kept as simple as possible for clarity and for focussing more on the fracture behavior. Therefore, additive decomposition of the strain into elastic and plastic components is chosen. The plastic slip field evolution is governed by the slip law,

$$\dot{\gamma}^\alpha = \dot{\gamma}_0^\alpha (|\tau^\alpha + \nabla \cdot \xi^\alpha|/s^\alpha)^{\frac{1}{m}} \text{sign}(\tau^\alpha + \nabla \cdot \xi^\alpha) \quad (1)$$

where $\tau^\alpha = \sigma : \mathbf{P}^\alpha$ is the resolved Schmid stress on the slip systems with $\mathbf{P}^\alpha = \frac{1}{2}(\mathbf{s}^\alpha \otimes \mathbf{n}^\alpha + \mathbf{n}^\alpha \otimes \mathbf{s}^\alpha)$, the symmetrized Schmid tensor, where \mathbf{s}^α and \mathbf{n}^α are the unit slip direction vector and unit normal vector on slip system α , respectively and ξ^α is the microstress vector $\xi^\alpha = \partial \psi_{\text{vp}} / \partial \nabla \gamma^\alpha = A \nabla \gamma^\alpha$ bringing the plastic slip gradients into the plasticity formulation. A is a scalar quantity, which includes an internal length scale parameter, and in this work it is defined as $A = ER^2/(16(1 - \nu^2))$ where R is a typical length scale for dislocation interactions. In these types of models the internal length scale could be related to different microstructural features and the value would vary, e.g. [31] relates it to dislocation spacing, and [32] to grain size. In this work we link the length scale parameters R to the average grain size. As derived in [33], the microscopic traction (associated with ξ) on the outer boundaries of the specimen is defined in terms of scalar microscopic traction χ^α that satisfies,

$$\chi^\alpha = \xi \cdot \bar{\mathbf{n}} \quad (2)$$

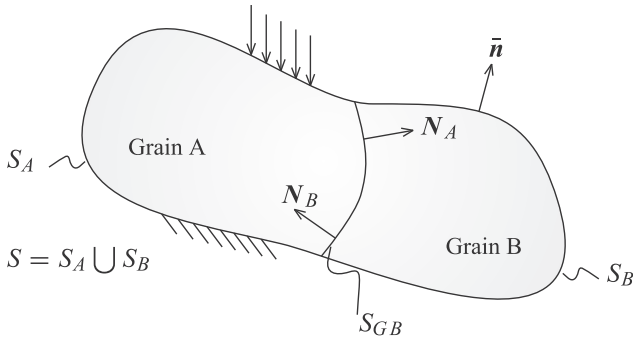


Fig. 1. A representative bi-crystal specimen with a grain boundary.

whereas the interfacial tractions λ_A^α and λ_B^α are defined along the grain boundaries and fulfill,

$$\lambda_A^\alpha = \xi \cdot N^A \quad (3)$$

$$\lambda_B^\alpha = \xi \cdot N^B \quad (4)$$

Please see Fig. 1 for the definition of \bar{n} , N^A and N^B .

For the solution of initial boundary value problems a fully coupled finite element solution algorithm is employed where both the displacement \mathbf{u} and the plastic slips γ^α are considered as primary variables. In the classical (local) crystal plasticity models the linear momentum balance equation is converted to a weak form and discretized into linear set of equations and solved incrementally where the displacement is the only degree of freedom. However in the current model the gradients of the plastic slips are required. Therefore the plastic slip field on each slip system are taken as global state variables. This results in a fully coupled model in terms of \mathbf{u} and γ^α . These fields are determined in the solution domain by solving simultaneously (monolithically) the linear momentum balance ($\nabla \cdot \boldsymbol{\sigma} = 0$) and the slip evolution Eq. (1) for $m = 1$ and constant slip resistance, which constitute the local strong form of the balance equations:

$$\begin{aligned} \nabla \cdot \boldsymbol{\sigma} &= \mathbf{0} \\ \dot{\gamma}^\alpha - \frac{\dot{\gamma}_0^\alpha}{s^\alpha} \tau^\alpha - \frac{\dot{\gamma}_0^\alpha}{s^\alpha} \nabla \cdot \boldsymbol{\xi}^\alpha &= 0 \end{aligned} \quad (5)$$

Note that the current choice of $m = 1$ introduces a high viscosity effect resulting in stabilization of any localization process. Yet, this preference is not based only on the regularization aspects but also gives a duality with models using a linear drag law for the dislocation motion to determine the slip. Other values of m or introducing a lower viscosity would affect the obtained results in the upcoming sections. For any quantitative analysis of metals, the parameters of the model and the value of the m should be identified accordingly. Since we conduct a qualitative analysis in the numerical examples section to illustrate the performance of the proposed models, we use the simplest choice for m value.

The variational expressions representing the weak forms of the governing equations given above are obtained through a multiplication by weighting functions $\delta_{\mathbf{u}}$ and δ_{γ^α} and integration over the domain Ω , which is subdivided into finite elements, where the unknown fields of the displacement and plastic slips and the associated weighting functions within each element are approximated by their nodal values multiplied with the interpolation shape functions. Then the weak forms of the balance equations are linearized with respect to the variations of the primary variables \mathbf{u} and γ^α and solved by means of a Newton-Raphson solution scheme for the increments of the displacement field $\Delta \mathbf{u}$ and the plastic slips $\Delta \gamma^\alpha$. The gradient nature of the model and the choice for a highly viscous case with $m = 1$, makes the model quite efficient and convergent. The procedure results in a system of linear equations which can be written in the following matrix format,

$$\begin{bmatrix} \mathbf{K}^{uu} & \mathbf{K}^{u\gamma} \\ \mathbf{K}^{\gamma u} & \mathbf{K}^{\gamma\gamma} \end{bmatrix} \begin{bmatrix} \Delta \mathbf{u} \\ \Delta \gamma^\alpha \end{bmatrix} = \begin{bmatrix} -\mathbf{R}^u + \mathbf{R}_u^{ext} \\ -\mathbf{R}^\gamma + \mathbf{R}_\gamma^{ext} \end{bmatrix} \quad (6)$$

where \mathbf{K}^{uu} , $\mathbf{K}^{u\gamma}$, $\mathbf{K}^{\gamma u}$ and $\mathbf{K}^{\gamma\gamma}$ represent the global tangent matrices while \mathbf{R}^u and \mathbf{R}^γ are the global residual columns. The contributions \mathbf{R}_u^{ext} and \mathbf{R}_γ^{ext} originate from the boundary terms. A detailed finite element implementation of the model as a user element in 2D is presented in [30]. Note that, the global degrees of freedom in this framework are the displacement and the plastic slips, in terms of which the boundary conditions are defined. There are two types of conditions that could be used at grain boundaries for plasticity during polycrystal simulations. Setting interfacial tractions λ^A and λ^B to zero leads to soft boundary conditions where the slips reaching to the grain boundary does not 'feel' the existence of the neighboring grain and/or resistance of the grain boundary. Obviously, this is one extreme end of the spectrum and on the other extreme end, by enforcing slips to be zero, hard boundary conditions can be imposed. This leads to the development of a boundary layer in terms of plastic slip and the related stress concentrations at the grain boundaries. The real behavior is expected to be in between these two extreme cases and in fact modeling of dislocation (slip) - grain boundary interaction is an active research problem on its own, (see e.g. [34,33]). In addition to these boundary conditions, the special case of continuous plastic slip across grain boundaries is also enforced and compared with the responses obtained by soft and hard boundary conditions. The realization of these conditions in the computational setting is briefly discussed at the end of the next section.

3. Cohesive zone modeling

The generalized potential-based constitutive model for mixed-mode cohesive fracture is employed here [27,28] in conjunction with physical parameters such as fracture energy, cohesive strength and shape of cohesive interactions. The mixed-mode nature of the model is important for the current study as the traction developing between the grains highly depend on the orientation of the grain boundary with respect to the loading and the misorientation of the grains. The model can characterize different fracture energies in each fracture mode, and it gives the freedom to use different traction-separation relations based on the used parameters. The potential has been named PPR (Park-Paulino-Roesler), after the first initials of the authors' last names.

As described in detail in [28], Fig. 2 presents the overview of the cohesive interactions of the PPR model. The normal cohesive interaction region is rectangular and bounded by δ_n and δ_t . Complete cohesive normal failure occurs when the normal separation, Δ_n , reaches the normal final crack opening width, δ_n , or the effective sliding displacement, Δ_t , reaches the tangential conjugate final crack opening width, δ_t . The tangential cohesive interaction is also rectangular and bounded by δ_t and δ_n . Complete cohesive tangential failure occurs when the effective sliding displacement reaches the tangential final crack opening width, δ_t , or normal separation reaches the normal conjugate final crack opening width, δ_n .

The shape parameters α and β govern the normal and tangential softening curve shapes. A shape parameter less than 2 causes plateau-type behavior, whereas a shape parameter greater than 2 yields behavior indicative of quasi-brittle materials. When Δ_n reaches the critical opening displacement, δ_{nc} , the normal cohesive traction is at its maximum, σ_{max} (the normal cohesive strength). When the sliding displacement reaches the critical sliding displacement, δ_{tc} , the effective tangential traction is at its maximum, τ_{max} (the tangential cohesive strength). The area under the normal cohesive interaction for $\Delta_t = 0$ corresponds to the normal fracture energy, ϕ_n , while the area under the tangential cohesive interaction for $\Delta_n = 0$ corresponds to the tangential fracture energy, ϕ_t .

The model is described through a potential in the following way,

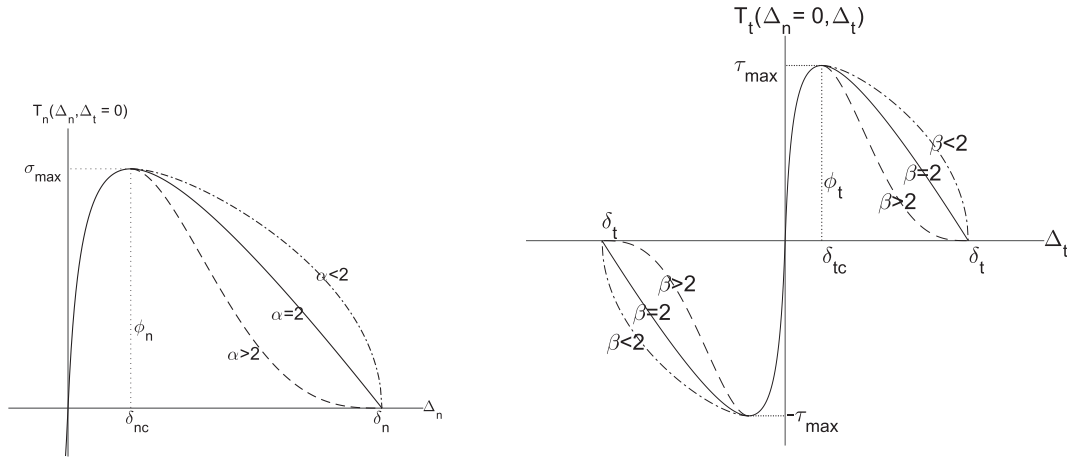


Fig. 2. Traction-separation relation of the PPR model [28].

Table 1
Slip systems used in the implementation.

Slip system	\vec{n}	\vec{s}
1	$\frac{1}{\sqrt{2}} \begin{bmatrix} 1 \\ 1 \\ 0 \end{bmatrix}$	$\frac{1}{\sqrt{3}} \begin{bmatrix} 1 \\ 1 \\ 1 \end{bmatrix}$
2	$\frac{1}{\sqrt{2}} \begin{bmatrix} 1 \\ 0 \\ 1 \end{bmatrix}$	$\frac{1}{\sqrt{3}} \begin{bmatrix} 1 \\ 1 \\ 1 \end{bmatrix}$
3	$\frac{1}{\sqrt{2}} \begin{bmatrix} 0 \\ 1 \\ 1 \end{bmatrix}$	$\frac{1}{\sqrt{3}} \begin{bmatrix} 1 \\ 1 \\ 1 \end{bmatrix}$
4	$\frac{1}{\sqrt{2}} \begin{bmatrix} 1 \\ 1 \\ 0 \end{bmatrix}$	$\frac{1}{\sqrt{3}} \begin{bmatrix} 1 \\ \bar{1} \\ 1 \end{bmatrix}$
5	$\frac{1}{\sqrt{2}} \begin{bmatrix} 0 \\ 1 \\ 1 \end{bmatrix}$	$\frac{1}{\sqrt{3}} \begin{bmatrix} 1 \\ 1 \\ 1 \end{bmatrix}$

$$\Psi(\Delta_n, \Delta_t) = \min(\Phi_n, \Phi_t) + \left[\Gamma_n \left(1 - \frac{\Delta_n}{\delta_n} \right)^\alpha \left(\frac{m}{\alpha} + \frac{\Delta_n}{\delta_n} \right)^m + \Phi_n - \Phi_t \right] \times \left[\Gamma_t \left(1 - \frac{|\Delta_t|}{\delta_t} \right)^\beta \left(\frac{n}{\beta} + \frac{|\Delta_t|}{\delta_t} \right)^n + \Phi_t - \Phi_n \right] \quad (7)$$

with constants

$$\Gamma_t = \begin{cases} \left(\frac{\alpha}{m} \right)^m, & \Phi_n < \Phi_t \\ -\Phi_n \left(\frac{\alpha}{m} \right)^m, & \Phi_n \geq \Phi_t \end{cases} \quad (8)$$

$$\Gamma_t = \begin{cases} \left(\frac{\beta}{n} \right)^n, & \Phi_t \leq \Phi_n \\ -\Phi_t \left(\frac{\beta}{n} \right)^n, & \Phi_t > \Phi_n \end{cases} \quad (9)$$

where

$$m = \frac{\alpha(\alpha - 1)\lambda_n^2}{1 - \alpha\lambda_n^2}, \quad n = \frac{\beta(\beta - 1)\lambda_t^2}{1 - \beta\lambda_t^2} \quad (10)$$

The gradients of the PPR potential lead directly to the traction vector,

$$T_n(\Delta_n, \Delta_t) = \frac{\Gamma_n}{\delta_n} \left[m \left(1 - \frac{\Delta_n}{\delta_n} \right)^\alpha \left(\frac{m}{\alpha} + \frac{\Delta_n}{\delta_n} \right)^{m-1} - \alpha \left(1 - \frac{\Delta_n}{\delta_n} \right)^{\alpha-1} \left(\frac{m}{\alpha} + \frac{\Delta_n}{\delta_n} \right)^m \right] \times \left[\Gamma_t \left(1 - \frac{|\Delta_t|}{\delta_t} \right)^\beta \left(\frac{n}{\beta} + \frac{|\Delta_t|}{\delta_t} \right)^n + \Phi_n - \Phi_t \right] \quad (11)$$

$$T_t(\Delta_n, \Delta_t) = \frac{\Gamma_t}{\delta_t} \left[n \left(1 - \frac{|\Delta_t|}{\delta_t} \right)^\beta \left(\frac{n}{\beta} - \frac{|\Delta_t|}{\delta_t} \right)^{n-1} - \beta \left(1 - \frac{|\Delta_t|}{\delta_t} \right)^{\beta-1} \left(\frac{n}{\beta} + \frac{|\Delta_t|}{\delta_t} \right)^n \right] \times \left[\Gamma_n \left(1 - \frac{\Delta_n}{\delta_n} \right)^\alpha \left(\frac{m}{\alpha} + \frac{\Delta_n}{\delta_n} \right)^m + \Phi_n - \Phi_t \right] \frac{\Delta_t}{|\Delta_t|} \quad (12)$$

Here, m, n are non-dimensional exponents, T_n is the normal cohesive traction, T_t is the tangential cohesive traction, α, β are shape parameters, λ_n, λ_t are initial slope indicators, Γ_n, Γ_t are energy constants, Δ_n is the normal separation, Δ_t is the effective sliding displacement, δ_t, δ_n are the normal and tangential final crack opening widths, Φ_n, Φ_t are fracture energies. For more details about the model see [27]. The interface element is equipped with 12 nodes which is compatible with 10-noded tetrahedra elements used for the discretization of grains. Corner nodes of both bulk and interface elements have 8 degrees of freedom (3 displacement components and 5 slip) and the mid-edge nodes have only displacement degrees of freedom, please see [33] for bulk element details. The formulation can be easily extended to host 12 slip systems (verified with low cost models) but currently 5 slip systems (all of them are octahedral slip systems) of a face centered cubic crystal given in Table 1 are used due to overwhelming computational cost. Although the interface element has slip degrees of freedom (dofs), the corresponding elements of the internal force column and the associated elements of the tangent stiffness matrix are set to zero. In other words, the interface elements do not contribute to the slip conservation equations (Eq. 2b) in any case. In case of hard boundary conditions along the grain boundaries, the slip dofs of the ‘upper’ and ‘lower’ faces of the interface elements are set to zero explicitly. In case of soft boundaries, the grain boundaries are traction free and the two faces of the interface elements are ‘disconnected’ in terms of slip dofs. In other words, slip dofs of the corresponding nodes of the ‘upper’ and ‘lower’ faces of interface elements attain different values. In case of continuous slips across grain boundaries (designated as continuous in the next section), equality constraint equations (tyings) are used to make the slip dofs of the corresponding nodes of the ‘upper’ and ‘lower’ faces equal.

Abaqus input files including the geometry, mesh, loading, solid elements, boundary conditions, grain boundary conditions, and the cohesive elements are prepared through developed scripts. The microstructure with grains are prepared with Neper open source software [35,38]. The interface elements are inserted between the grains automatically through developed scripts. The user element subroutines for plasticity and cohesive zone model are run together using the input files. The obtained results are converted to Abaqus odb files using the developed scripts. Various numerical examples are presented and discussed in the following section in order to illustrate the performance of the PPR cohesive zone approach for the inter-granular crack initiation and propagation in realistic microstructures.

4. Numerical observations

For the bulk behavior of each grain the mixed finite element formulation is employed to obtain the plasticity evolution. The plastic slips evolve on each slip system in a rate dependent matter through the projected stress and the higher order nonlocal stress term, which depends on the gradient of the plastic slip itself, i.e. the geometrically necessary dislocation densities. Since the plastic slip values are taken as the primary variables of the finite element solution scheme, it is quite straightforward to obtain their gradients or the GND densities through shape functions. The discretization is conducted by 10-node tetrahedra elements with quadratic interpolation for the displacement field and linear interpolation for the slips. The microstructure with random grain orientations are obtained through Voronoi tessellation method with the help of the Neper software.

Due to the orientation difference among grains, the incompatibility of the deformation at the grain boundaries results in stress concentrations, which increases in each increment and gives rise to the traction on these boundaries. The incorporated PPR cohesive zone elements work between the grains and take into account the degradation due to the increase in the traction values. All the information regarding the coupled grain interior finite elements working with strain gradient crystal plasticity, the inter-granular cohesive zone elements, the geometry and meshing of the microstructure is included in the input files for Abaqus simulations which prepared automatically through developed scripts. Throughout the solution procedure user element subroutine for the strain gradient crystal plasticity for the bulk material behavior and the user element subroutine file for the PPR cohesive zone model [28] are run together. Due to the gradient and viscous nature of the plasticity model the localizations and stress concentrations are handled easily and there has been no numerical convergence issues in the simulations.

The numerical examples address the effect of orientation distribution, specimen size, grain boundary conditions and the fracture energy on the inter-granular crack initiation, propagation and the toughness of the material. In this regard this would be a unique study where micro nonlocal plasticity is combined with cohesive zone modeling approach to illustrate inter-granular cracking in micron sized specimens. In all examples a cylindrical specimen is considered under uniaxial loading with the material parameters presented in Table 2 for plasticity and Table 3 for cohesive zone model. An example microstructure with the boundary conditions, mesh and the loading is presented in Fig. 3. In all cases 5 slip systems are considered to be active within each grain. For all analysis presented in the following sub-sections, at the two circular ends of the specimen, hard boundary conditions are imposed whereas the slips can freely reach the lateral surface which corresponds to soft boundary conditions.

In the following subsections detailed numerical results will be presented in order to illustrate the performance of the developed model.

4.1. Orientation distribution dependence

The specimen has a length of 100 μm and diameter 25 μm and has 32 randomly oriented grains. The first example studies both micro and macro responses of the orientation distribution on the fracture behavior of the material with soft boundary conditions along the grain

Table 2
Material properties of the strain gradient crystal plasticity model.

Young modulus E [MPa]	Poisson ratio ν []	Reference slip rate $\dot{\gamma}_0$ [s^{-1}]	Slip resistance s [MPa]	Orientations [°]	Material length scale R [μm]
70000.0	0.33	0.115	25.0	Random	0.4

Table 3
Material properties of the cohesive zone element.

Normal and tangential fracture energy Φ_n, Φ_t [N/m]	Normal and tangential cohesive traction T_n, T_t [MPa]	Shape parameters α, β []	Initial slop indicators λ_n, λ_t
60	60.0	2.0	0.005

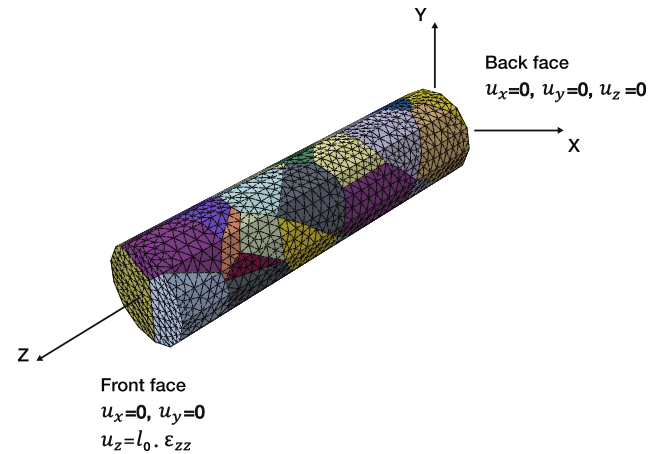


Fig. 3. Boundary conditions and loading on the microstructure.

boundaries. In all cases the material have the same pole figure since the set of orientation assigned to the grains is exactly same. However in each example the distribution is randomly altered. In this way we will illustrate that the crack initiation location and the toughness of the material can actually be different for the same microstructure having same pole figure (texture) but different orientation distribution.

Figs. 4 and 5 show the stress and strain distribution respectively, in the loading direction just before the softening starts. It is clearly illustrated that the spatial evolution of the stress and strain depend on the orientation of the grains, which is captured intrinsically through the used strain gradient crystal plasticity framework. The evolution of different plastic strains in each grain results in stress concentrations at the grain boundaries, which is one of the most important fracture damage and fracture mechanisms at this length scale. The traction at the grain boundaries depends on the orientation mismatch as well as the shape and the orientation of the grain boundaries. Even though certain grains are prone to high traction and crack initiation due to their orientation with respect to loading, the random distribution of the orientation set results in a completely different fracture behavior as illustrated in Fig. 6 for the moment where the macroscopic stress drops to zero. In each of the figures the crack is initiated at a different location. The macroscopic behavior is affected by this phenomenon as well as shown in Fig. 7. The stress strain response and the toughness in each case are completely different even though the material parameters, loading and the texture are exactly same. This is a statistical effect specific to the current length scale and it could only be simulated through a micromechanically motivated plasticity framework combined with a proper crack initiation and propagation model. Random orientation distribution with different pole figures would naturally lead to random crack initiation. However in this example the orientations are picked from the same set with a different distribution. The obtained results are quite natural considering the physics of the problem and the capability of the models. However it is a unique study showing this phenomenon and it offers the possibility of conducting physical simulations for microforming processes in a commercial software, which is quite user friendly.

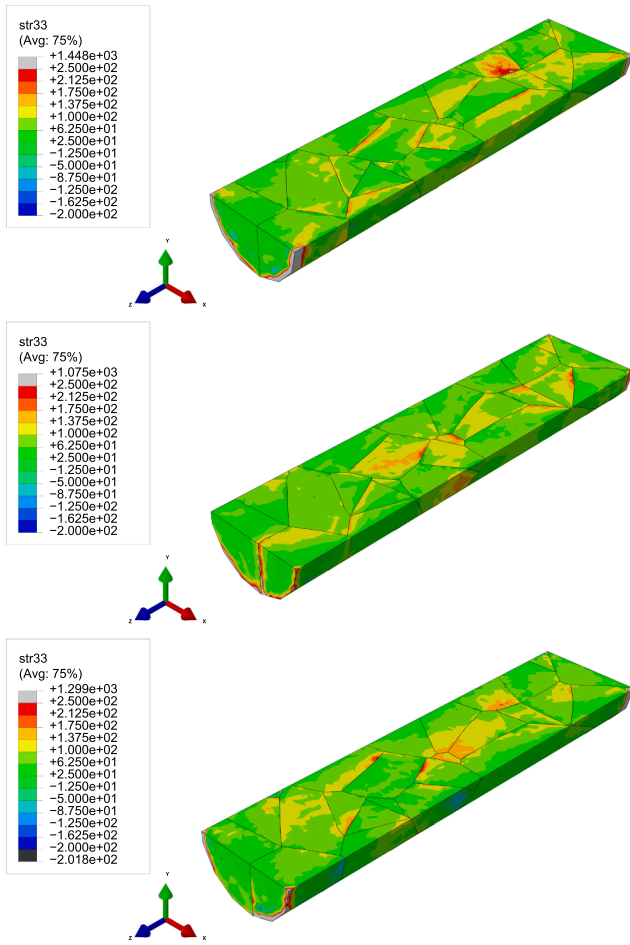


Fig. 4. Stress distribution before cracking for different orientation distributions.

4.2. Boundary condition dependence

In the next example, the effect of the boundary conditions on the plasticity and fracture behavior of micron sized specimens is addressed in detail. The finite element framework of the plasticity model used in this study allows us to describe boundary conditions at the grain boundaries in terms of plastic slip, which is unique to such higher order non-local crystal plasticity models. The classical crystal plasticity theories do not handle the boundaries properly and they would lead to jumps in terms of plastic slips. The classical approach is not physical enough concerning the grain boundaries, yet it is commonly used to capture the anisotropic behavior at grain scale. For a more micro-mechanically motivated simulation, the dislocation-grain boundary interaction should be addressed in a more physical way. Therefore various studies have started to concentrate on such interaction (see e.g. [37,34,33,38–40]) mechanisms. The incorporation of such models into higher order non-local crystal plasticity frameworks is quite demanding and in many cases the studies are restricted to simple bi-crystal studies or simple microstructures. Moreover, the attention has been basically focused on the localization at the grain boundaries rather than crack initiation and propagation. In current work, fracture phenomenon is addressed in a more complicated microstructure and the dislocation-grain boundary interactions are handled through solely limiting cases such as free slip (micro-free), hard boundary (zero slip) and continuous slip conditions, which means the free transfer of dislocations through the grain boundaries, complete blockage of dislocations and continues transfer of dislocations at the GBs respectively. Even though the description is not complicated and it does not involve orientation mismatch function with a GB strength parameter, it is still able to describe

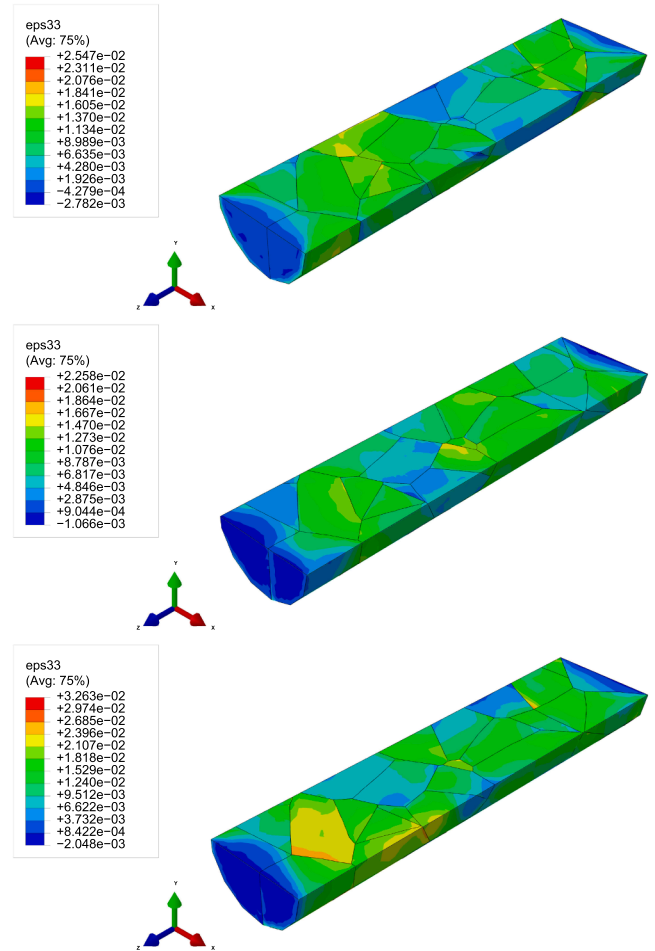


Fig. 5. Strain distribution before cracking for different orientation distributions.

more physics of the problem.

In Fig. 8 the spatial stress (σ_{zz}) distribution is presented for soft, continuous and hard grain boundary conditions at certain loading histories just before the softening starts. At the hardening phase of the loading the stress concentrations at the grain boundaries are highest for the hard boundary condition case, followed by the continuous and soft cases. which can be observed from the macroscopic response presented in Fig. 9 as well. Therefore the cracks are initiated first at multiple locations in the hard boundary case and the material starts to soften while the other two cases are still hardening. In short time the other two cases starts to soften as well in a similar way. Even though the initial crack locations might depend on the boundary condition the complete failure occurs at the same location which was illustrated in the 1st orientation distribution case presented in Fig. 6. Hard boundary conditions make the specimen more prone to failure and lead to minimum toughness. The complete fracture occurs with substantially low ductility for hard grain boundary condition case followed by the continuous grain boundary condition. For the case of soft boundary condition much higher plastic strain levels are obtained before the failure. In Fig. 10 the first two slip systems out of 5 are plotted on a plane passing through the center. It can be seen that the hard boundary condition clearly enforces the slip values to be zero at the grain boundaries. This is a quite strong condition and keeps the plastic strain value quite low in the grains. In the continuous case the continuity is enforced at the grain boundaries which relaxes the evolution of the plastic strain. In the case of the soft boundary conditions serious jumps in the plastic slip values are obtained. The plasticity evolves easily and the stress concentrations are considerably less than the other cases. The toughness of the material is

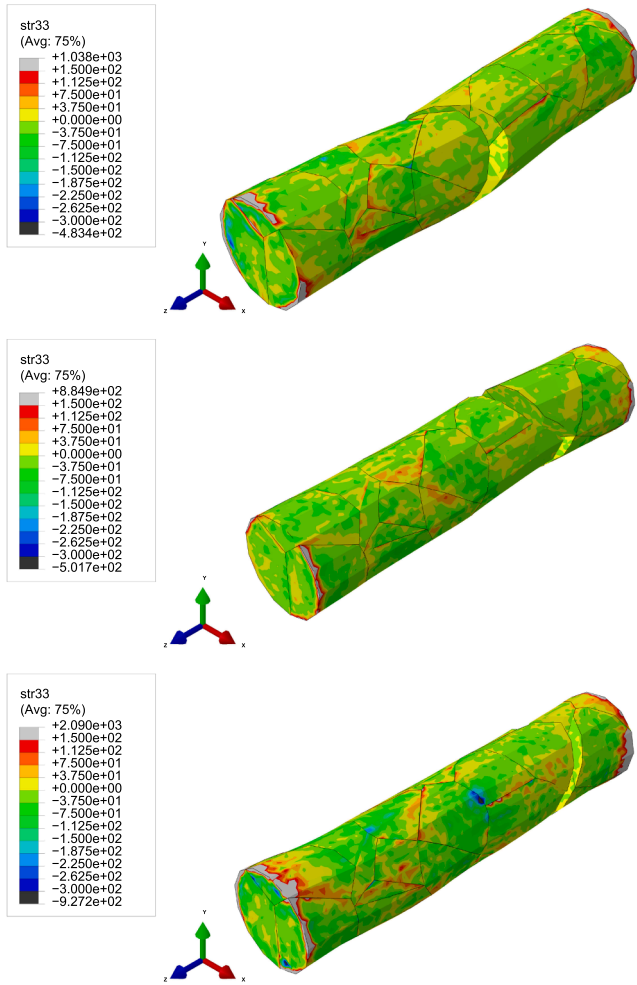


Fig. 6. Stress distribution after cracking for different orientation distributions.

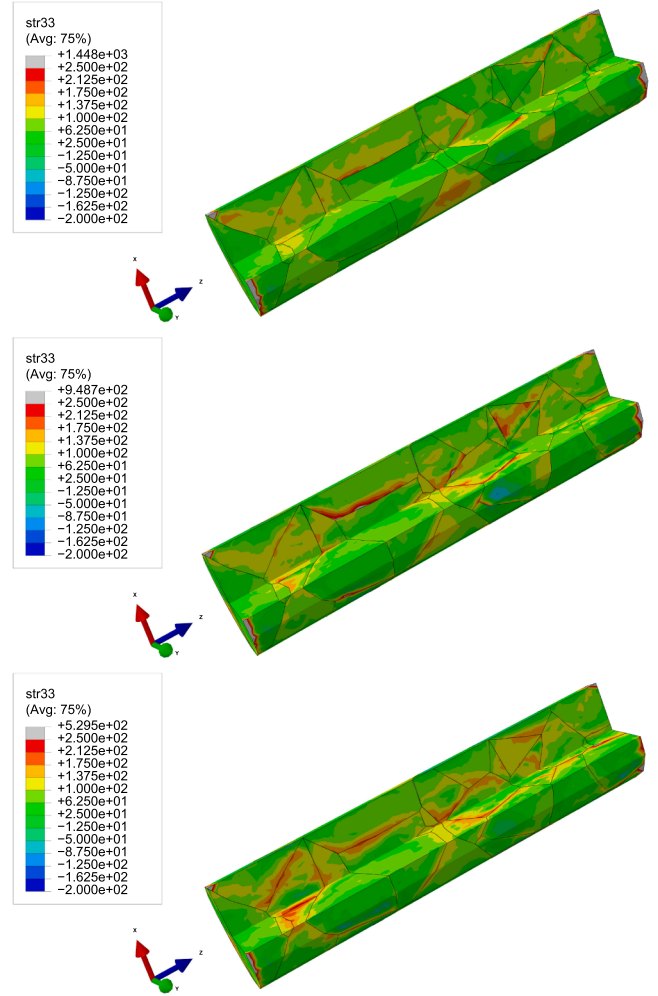


Fig. 8. Stress distribution for soft (top), continuous (middle) and hard (bottom) boundary condition cases before the crack occurs.

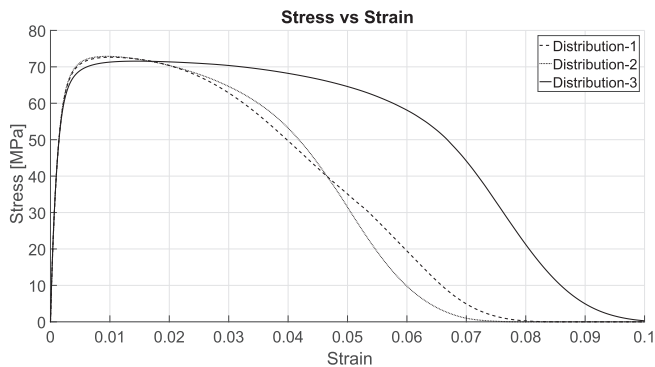


Fig. 7. Stress vs. strain plot for different orientation distributions.

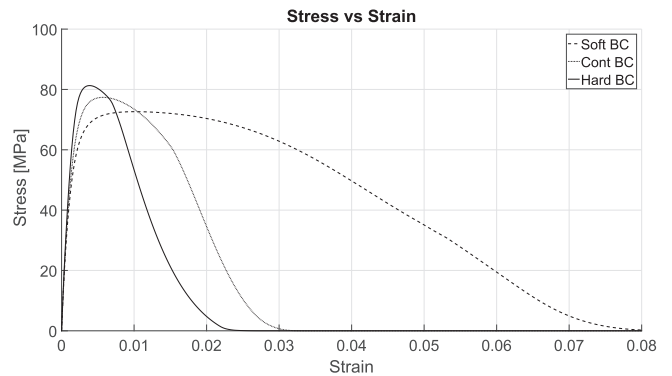


Fig. 9. Stress vs. strain plot for different boundary conditions.

maximum for the case with soft grain boundary conditions allowing free evolution of the slip at the boundary.

4.3. Size effect

In this example the effect of the specimen size on the plasticity and the fracture behavior of micron sized specimens is addressed shortly. The smaller specimen considered here has 48 μm length and 12 μm diameter and has soft grain boundary conditions, while the bigger one has 100 μm length and 25 μm diameter. In Fig. 11 the spatial distribution of the stress is illustrated before and after failure, which shows similar trend with the large specimen. As it can be seen in the

macroscopic response curves in Fig. 12 as well, for the hardening plasticity range the stress values are higher for the small specimen, which is an expected result for strain gradient crystal plasticity framework. Yet, the softening starts earlier in the small specimen and failure occurs for much smaller macroscopic strain values. Moreover, the toughness is higher for the large specimen. Note that in these observations only the specimen size has been changed while all the other plasticity and fracture parameters are kept same. It is concluded that while the yield strength is higher for the smaller specimen the toughness of the material is smaller.

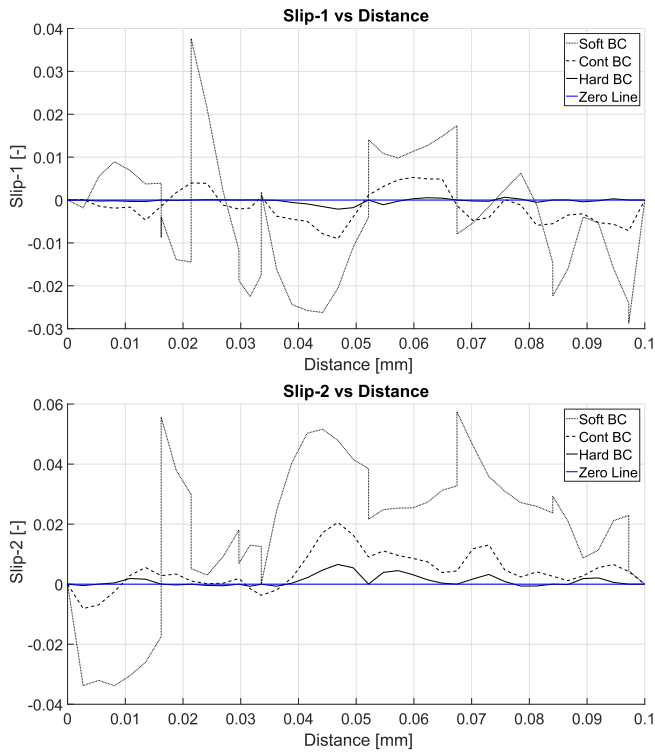


Fig. 10. Slip-1 and Slip-2 values along the center of the specimen.

4.4. Fracture energy dependence

In the previous examples the normal and tangential fracture energy parameters are kept fixed as $\Phi_n = 60 \text{ J/m}^2$ and $\Phi_t = 60 \text{ J/m}^2$ in order to analyze orientation distribution, grain boundary condition and size dependent behavior. In here, the effect of the fracture energy parameters Φ_n and Φ_t are addressed on both macro and micro responses considering soft boundary conditions on the first orientation distribution case where the specimen dimensions are taken as $100 \mu\text{m}$ length and $25 \mu\text{m}$ diameter. In this context different fracture energy parameters are considered, i.e. $\Phi_n = \Phi_t = 75, 150$ and 250 J/m^2 . Increasing the fracture energy parameter in the cohesive zone relation would result in a more ductile failure mechanism at the grain boundary interfaces, which would lead to an increase in the macroscopic ductility of the material as well. Fig. 14 illustrates the strain distribution at the states where stress drops to zero for 75 J/m^2 and 150 J/m^2 . For 250 J/m^2 case the same deformation state is considered with 150 J/m^2 to have a comparison in the macroscopic behavior. At the low fracture energy parameter levels the elongation of the specimen is quite low before the fracture initiation. For the high values of the parameter considerable energy is dissipated plastically all over the specimen and high values of elongation is obtained before the initiation of the crack. Therefore this parameter affects substantially the global ductile failure of the material. The macroscopic stress versus strain behavior is illustrated in Fig. 13, where the effect of the parameter is clearly shown.

5. Conclusion and discussion

This paper addresses the modeling of inter-granular fracture of micron sized specimens through strain gradient crystal plasticity and cohesive zone modeling approaches. It is one of the unique studies illustrating clearly the effect of microstructural features on the fracture performance of the materials at this length scale. Even though the inter-

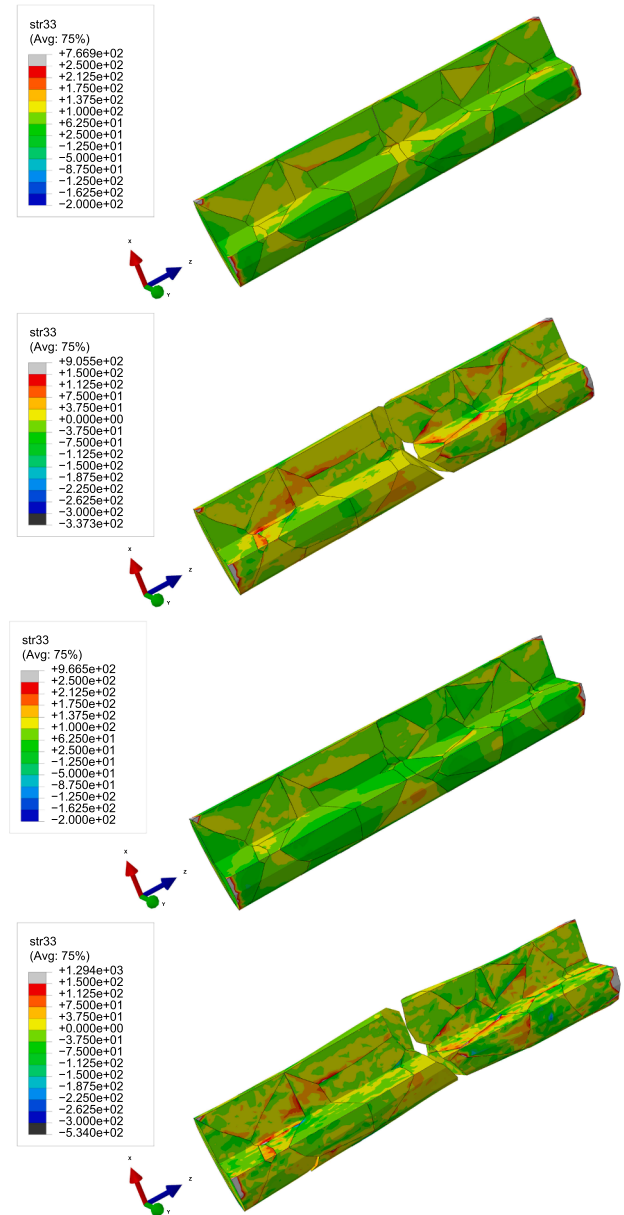


Fig. 11. Size effect illustration for small (a–b) and large (c–d) specimen before and after crack occurs.

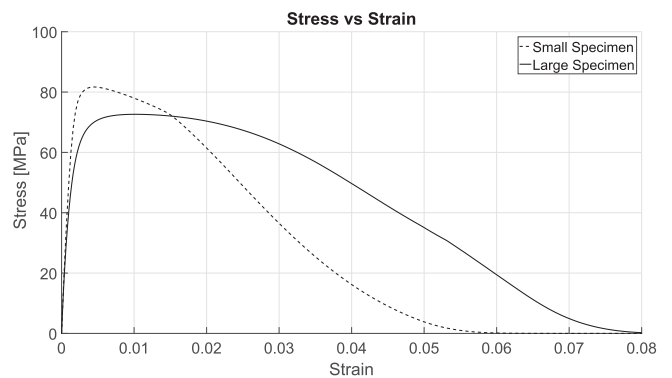


Fig. 12. Stress vs. strain relations for small and large specimens.

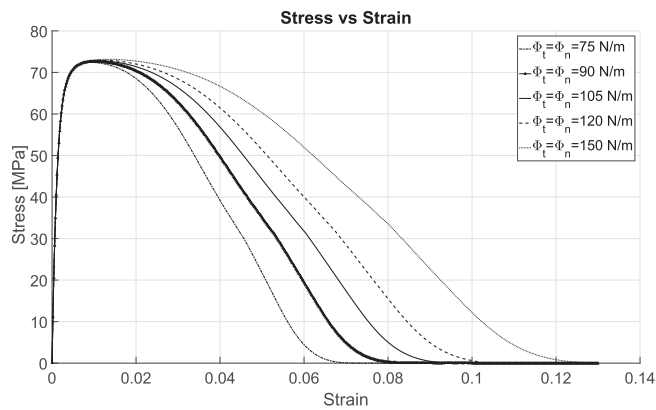


Fig. 13. Stress vs. strain relations for different fracture energy parameter values.

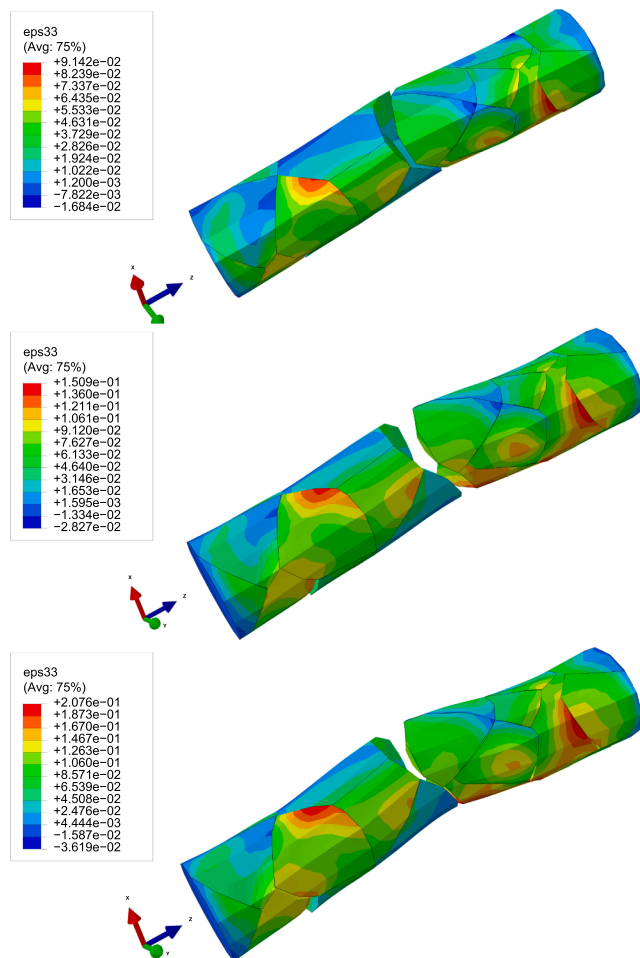


Fig. 14. Strain distribution after cracking for fracture energy parameter values of 75 J/m², 150 J/m² and 250 J/m².

granular fracture is regarded dominantly as a brittle fracture mechanism certain high strength aerospace alloys exhibit this type of ductile cracking. However, the link between the microstructure evolution and the fracture is missing in the literature. The previous studies focused more on the phenomenological modelling of this type of degradation due to the difficulty of combining different complicated user finite element models. The study shows explicitly the orientation distribution, size and grain boundary condition dependent plasticity, fracture and toughness behavior of these materials. The current work stays at the qualitative analysis level and it does not refer to a specific

material at the moment. However the developed model offers a great potential to be used in the modeling of micromechanical ductile fracture and the modeling of specific materials would be a matter of material parameter identification. It is important to note that even though the plasticity model used in the grains is physics based, the cohesive zone relations are purely phenomenological as used in many other studies for crack initiation and propagation at the interfaces. As a next step the study will be extended by implementing physics based traction-separation relations that can properly describe the ductile failure mechanisms at the grain boundaries (see e.g. [41,42]). Such description will be based on the growth of pores leading to ductile fracture at the interfaces.

Compliance with ethical standards

Funding: This study was funded by Scientific and Technological Research Council of Turkey (TÜBİTAK) (Grant No. 117M106).

Declaration of Competing Interest

The authors declare that they have no conflict of interest.

Acknowledgments

Tuncay Yalçinkaya gratefully acknowledges the support by the Scientific and Technological Research Council of Turkey (TÜBİTAK) under the 3501 Programme (Grant No. 117M106).

References

- [1] T. Yalçinkaya, A. Demirci, I. Simonovski, I. Özdemir, Micromechanical modelling of size effects in microforming, *Procedia Eng.* 207 (2017) 998–1003.
- [2] T. Yalçinkaya, I. Özdemir, I. Simonovski, Micromechanical modeling of intrinsic and specimen size effects in microforming, *Int. J. Mater. Form.* 11 (2018) 729–741.
- [3] G. Cailletaud, S. Forest, D. Jeulin, F. Feyel, I. Galliet, V. Mounoury, S. Quilici, Some elements of microstructural mechanics, *Comp. Mater. Sci.* 27 (3) (2003) 351–374.
- [4] P. Zhang, M. Karimpour, D. Balint, J. Lin, Cohesive zone representation and junction partitioning for crystal plasticity analyses, *Int. J. Numer. Meth. Eng.* 92 (8) (2012) 715–733.
- [5] B. Güler, Ü. Simsek, T. Yalçinkaya, M. Efe, Grain-scale investigations of deformation heterogeneities in aluminum alloys, *AIP Conf. Proc.* 1960 (2018) 170005.
- [6] G.M. Ludtka, D.E. Laughlin, The influence of microstructure and strength on the fracture mode and toughness of 7xxx series aluminum alloys, *Metall. Trans. A* 13 (1982) 411–425.
- [7] A. Pineau, A.A. Benzerga, T. Pardoen, Failure of metals i: Brittle and ductile fracture, *Acta Mater.* 107 (2016) 424–483.
- [8] T. Pardoen, D. Dumont, A. Deschamps, Y. Brechet, Grain boundary versus trans-granular ductile failure, *J. Mech. Phys. Solids.* 51 (2003) 637–665.
- [9] D. Dumont, A. Deschamps, Y. Brechet, A model for predicting fracture mode and toughness in 7000 series aluminium alloys, *Acta Mater.* 52 (2004) 2529–2540.
- [10] T. Pardoen, T.J. Massart, Interface controlled plastic flow modelled by strain gradient plasticity theory, *C.R. Mecanique.* 340 (2012) 247–260.
- [11] M. Fourmeau, C.D. Marioara, T. Borvik, A. Benallal, O.S. Hopperstad, A study of the influence of precipitate-free zones on the strain localization and failure of the aluminium alloy AA7075-T651, *Philos. Mag.* 95 (2015) 3278–3304.
- [12] S. Osovski, A. Srivastava, J.C. Williams, A. Needleman, Grain boundary crack growth in metastable titanium β alloys, *Acta Mater.* 82 (2015) 167–178.
- [13] H. Li, D. Huang, M. Zhan, Y. Li, X. Wang, S. Chen, High-temperature behaviors of grain boundary in titanium alloy: modeling and application to microcrack prediction, *Comput. Mater. Sci.* 140 (2017) 159–170.
- [14] A.K. Vasudevan, R.D. Doherty, Grain boundary ductile fracture in precipitation hardened aluminum alloys, *Acta Metall.* 35 (1987) 1193–1219.
- [15] T.H. Sanders, E.A. Starke, The relationship of microstructure to monotonic and cyclic straining of two age hardening aluminum alloys, *Metall. Trans. A* 7 (1976) 1407–1418.
- [16] N.U. Deshpande, A.M. Gokhale, D.K. Denzer, J. Liu, Relationship between fracture toughness, fracture path, and microstructure of 7050 aluminum alloy: Part I. Quantitative characterization, *Metall. Matter. Trans. A* 29 (1998) 1191–1201.
- [17] A.M. Gokhale, N.U. Deshpande, D.K. Denzer, J. Liu, Relationship between fracture toughness, fracture path, and microstructure of 7050 aluminum alloy: Part II. Multiple micromechanisms-based fracture toughness model, *Metall. Matter. Trans. A* 29 (1998) 1203–1210.
- [18] Y.J. Wei, L. Anand, Grain-boundary sliding and separation in polycrystalline metals: application to nanocrystalline fcc metals, *J. Mech. Phys. Solids.* 52 (2004) 2587–2616.
- [19] V. Yamakov, E. Saether, D.R. Phillips, E.H. Glaesgen, Molecular-dynamics

- simulation-based cohesive zone representation of intergranular fracture processes in aluminum, *J. Mech. Phys. Solids* 54 (2006) 1899–1928.
- [20] M. Paggi, E. Lehmann, C. Weber, A. Carpinteri, P. Wriggers, M. Schaper, A numerical investigation of the interplay between cohesive cracking and plasticity in polycrystalline materials, *Comput. Mater. Sci.* 77 (2013) 81–92.
- [21] I. Benedetti, M.H. Aliabadi, A three-dimensional cohesive-frictional grain-boundary micromechanical model for intergranular degradation and failure in polycrystalline materials, *Comput. Method Appl. Mech. Eng.* 265 (2013) 36–62.
- [22] A.C. Magee, L. Ladani, Representation of a microstructure with bimodal grain size distribution through crystal plasticity and cohesive interface modeling, *Mech. Mater.* 82 (2015) 1–12.
- [23] G. Geraci, M.H. Aliabadi, Micromechanical boundary element modelling of transgranular and intergranular cohesive cracking in polycrystalline materials, *Eng. Fract. Mech.* 176 (2017) 351–374.
- [24] T. Yalçinkaya, W.A.M. Brekelmans, M.G.D. Geers, Deformation patterning driven by rate dependent non-convex strain gradient plasticity, *J. Mech. Phys. Solids* 59 (2011) 1–17.
- [25] T. Yalçinkaya, Multi-scale modeling of microstructure evolution induced anisotropy in metals, *Key Eng. Mater.* 554 (2013) 2388–2399.
- [26] B. Klusemann, T. Yalçinkaya, Plastic deformation induced microstructure evolution through gradient enhanced crystal plasticity based on a non-convex helmholtz energy, *Int. J. Plasticity* 48 (2013) 168–188.
- [27] K. Park, G.H. Paulino, J.R. Roesler, A unified potential-based cohesive model of mixed-mode fracture, *J. Mech. Phys. Solids* 57 (2009) 891–908.
- [28] A. Cerrone, P. Wawrzynek, A. Nonn, G.H. Paulino, A. Ingrassia, Implementation and verification of the Park-Paulino-Roesler cohesive zone model in 3d, *Eng. Fract. Mech.* 120 (2014) 26–42.
- [29] T. Yalçinkaya, W.A.M. Brekelmans, M.G.D. Geers, Non-convex rate dependent strain gradient crystal plasticity and deformation patterning, *Int. J. Solids Struct.* 49 (2012) 2625–2636.
- [30] T. Yalçinkaya, Strain gradient crystal plasticity: thermodynamics and implementation, in: G. Voyiadjis (Ed.), *Handbook of Nonlocal Continuum Mechanics for Materials and Structures*, 2016, pp. 1001–1035.
- [31] W.D. Nix, H. Gao, Indentation size effects in crystalline materials: a law for strain gradient plasticity, *J. Mech. Phys. Solids* 46 (1998) 411–425.
- [32] G.Z. Voyiadjis, R.K. Abu Al-Rub, Gradient plasticity theory with a variable length scale parameter, *Int. J. Solids Struct.* 42 (2005) 3998–4029.
- [33] I. Özdemir, T. Yalçinkaya, Strain gradient crystal plasticity: Intergranular microstructure formation, in: G. Voyiadjis (Ed.), *Handbook of Nonlocal Continuum Mechanics for Materials and Structures*, 2017, pp. 1035–1065.
- [34] I. Özdemir, T. Yalçinkaya, Modeling of dislocation-grain boundary interactions in a strain gradient crystal plasticity framework, *Comput. Mech.* 54 (2014) 255–268.
- [35] R. Quey, P. Dawson, F. Barbe, Large-scale 3d random polycrystals for the finite element method: generation, meshing and remeshing, *Comput. Method Appl. Mech. Eng.* 200 (17) (2011) 1729–1745.
- [38] R. Quey, Neper: a 3d random polycrystal generator for the finite element method. version 3.3.0, 2018, <http://neper.sourceforge.net>.
- [37] M.E. Gurtin, A theory of grain boundaries that accounts automatically for grain misorientation and grain-boundary orientation, *J. Mech. Phys. Solids* 56 (2008) 640–662.
- [38] P.R.M. van Beers, V.G. Kouznetsova, M.G. Geers, Grain boundary interfacial plasticity with incorporation of internal structure and energy, *Mech. Mater.* 90 (2015) 69–82.
- [39] E. Bayerschen, A.T. McBride, B.D. Reddy, T. Böhlke, Review on slip transmission criteria in experiments and crystal plasticity models, *J. Mater. Sci.* 51 (2016) 2243–2258.
- [40] D. Gottschalk, A.T. McBride, B.D. Reddy, A. Javili, P. Wriggers, C.B. Hirschberger, Computational and theoretical aspects of a grain-boundary model that accounts for grain misorientation and grain-boundary orientation, *Comput. Mater. Sci.* 111 (2016) 443–459.
- [41] T. Yalçinkaya, A. Cocks, Physics based formulation of a cohesive zone model for ductile fracture, *Key Eng. Mat.* 651–653 (2015) 993–999.
- [42] T. Yalçinkaya, A. Cocks, Micromechanical cohesive zone relations for ductile fracture, *Procedia Struct. Integrity* 2 (2016) 1716–1723.